The behaviour of positron clouds in the single-particle regime under the influence of rotating wall electric fields

2012 New J. Phys. 14 075022

(http://iopscience.iop.org/1367-2630/14/7/075022)

New Journal of Physics
The open-access journal for physics

The behaviour of positron clouds in the single-particle regime under the influence of rotating wall electric fields

D P van der Werf[1], C A Isaac, C J Baker, T Mortensen, S J Kerrigan and M Charlton

Department of Physics, College of Science, Swansea University, Singleton Park, Swansea SA2 8PP, UK
E-mail: D.P.van.der.Werf@Swansea.ac.uk

New Journal of Physics **14** (2012) 075022 (14pp)
Received 7 March 2012
Published 25 July 2012
Online at http://www.njp.org/
doi:10.1088/1367-2630/14/7/075022

Abstract. Positron clouds are compressed following accumulation in a Surko-type two-stage buffer gas trap using an asymmetric rotating wall electric field. An analytic theory used to describe measurements of the rate of compression is discussed. Furthermore, we describe measurements taken without the rotating wall applied and with the rotating wall compression present during accumulation of the positron cloud. This has enabled total loss rates for the positrons via annihilation and collisional-induced radial transport to be isolated, with the latter mechanism found to be dominant. We have shown that the application of the rotating wall at a resonant frequency virtually eliminates radial transport, such that the positron loss is caused by annihilation in the gas.

[1] Author to whom any correspondence should be addressed.

Contents

1. Introduction

The accumulation and manipulation of low-energy positrons using buffer gas-based devices, pioneered by Surko and co-workers [1–3], is now routine in many laboratories around the world; see, e.g., [4–6]. The ability to accumulate large numbers of positrons has proved crucial in efforts to produce cold and trapped antihydrogen [7–13] and to provide large instantaneous fluxes of positrons in the study of systems containing more than one positronium atom [14, 15].

Positrons are typically stored in a Penning–Malmberg-type trap, into which they fall and are then cooled, via collisions with a buffer gas, typically molecular nitrogen as is used in the present study. In these traps, electrical potentials applied to cylindrical electrodes provide confinement of the particles along the axis of the instrument, whereas radial confinement is provided by an axial magnetic field, $\boldsymbol{B}$, typically of strength greater than several hundreds of Gauss. Under certain conditions, usually when the accumulator has three stages, with each stage held at a lower pressure than the one preceding it, positron lifetimes can range from tens to hundreds of seconds and many millions of them can be collected. Here, the positron cloud can be sufficiently dense, i.e. the Debye screening length is much smaller than the cloud dimensions, to form a so-called single-component plasma [1, 8, 16, 17]. Once in this state the combination of the radial self-electric field of the plasma and the applied magnetic field causes the plasma to rotate about the axis of the system with a constant angular frequency, $\omega_d = n_e q/2\epsilon_o B$, where n_e is the plasma density and q and ϵ_o are the charge of the particles and the vacuum dielectric constant, respectively.

Many devices that can be used to store single-component electron and positron plasmas (see e.g. [18] for descriptions of recent studies) have a section which contains an electrode that is azimuthally split into several (typically 4) segments. It has been known for some time that using these electrodes to apply a rotating electric field can arrest plasma expansion or even actively compress the cloud [19–24]. The precise mechanism for this need not concern us here, but the rotating wall is typically applied at a frequency greater than $\omega_d/2\pi$ and in the same sense as the natural rotation of the plasma, and to achieve compression some form of active cooling of the trapped particles is required. The latter, for instance for positrons, can be provided in high-magnetic-field (typically >1 T) systems by the emission of synchrotron radiation [8] or otherwise by the addition of a cooling gas to the system [5, 21].

The common feature of all these studies is that the positrons must be in the plasma state for the rotating wall to be effective. Indeed, early work with the ATHENA positron accumulator [25] showed that application of the rotating wall (at a frequency appropriate for plasma compression) in the pre-plasma stage of accumulation had a deleterious effect on the accumulation rate.

However, pioneering work by Greaves and co-workers [5, 26] has shown that a rotating wall can be used to compress a cloud of positrons in the so-called single-particle (i.e. pre-plasma) regime. That work demonstrated that application of a rotating wall of frequency at, or close to, the axial bounce frequency of the particles in the trap, $\omega_z = (qV_t/md_t^2)^{1/2}$, where V_t and d_t are trap parameters, respectively the electrical depth and length of the trap, and m is the mass, results in a compression of a positron cloud. Increases in central density of the cloud by a factor of about 100 were achieved [26].

This new technique holds promise for applications in positron accumulation, and in particular, for two-stage accumulators (see, e.g., [4–6]). These instruments are significantly cheaper and easier to operate than three-stage devices, which typically require a large electromagnet [1, 8] or a superconducting solenoid [5] for their operation. They are, for instance, beginning to find applications in atomic physics [27], where they can be used to provide narrow energy width beams [28] for the new field of high-resolution positron scattering.

Motivated by the work of Greaves and Moxom [26], we developed a new theory explaining single-particle compression in terms of sideband cooling [29]. Measurements on positron clouds, using the modified Swansea two-stage accumulator [4] that incorporates a split electrode as a means of introducing the rotating wall, corroborated the theory. The compression measurements were carried out on a cloud of positrons *after* the accumulation process was halted. In this paper, we will expand upon that work by studying the effect of applying the rotating wall during accumulation and also by investigating the role of different cooling gases. The remainder of the paper is organized as follows. Section 2 will briefly summarize the compression theory, whereas in section 3 we provide details of our apparatus and techniques. Results and discussion will be presented in section 4, followed by the concluding remarks in section 5.

2. Theory

Charged particles in an ideal Penning trap are radially confined by a magnetic field, $\boldsymbol{B} = B\hat{\mathbf{z}}$, where the z-axis is the axis of cylindrical symmetry, and axially by the potential

$$\phi(z, r) = \frac{m}{q}\frac{\omega_z^2}{2}\left(z^2 - \frac{r^2}{2}\right). \tag{1}$$

For a zero potential, i.e. $\omega_z = 0$, the particle only experiences a magnetic force and will exhibit a so-called cyclotron motion with frequency $\Omega_c = qB/m$, superposed on a constant velocity in the z-direction. Adding the Penning trap potential given by equation (1) changes the constant velocity into an axial bounce motion with frequency ω_z and gives rise to $\boldsymbol{E} \times \boldsymbol{B}$ fields, which modify Ω_c into ω_+, and cause the particle to exhibit magnetron motion with a frequency ω_- (also called ω_m). These frequencies are given by $\omega_\pm = \frac{1}{2}(\Omega_c \pm \sqrt{\Omega_c^2 - 2\omega_z^2})$. Typically,

$$\omega_+ \gg \omega_z \gg \omega_- \tag{2}$$

for a trapped particle.

The application of a rotating wall electric dipole field, asymmetric in the z-direction, can be described by adding a rotating wall potential to equation (1), resulting in

$$\phi(z, r, \theta) = \frac{m}{q}\frac{\omega_z^2}{2}\left(z^2 - \frac{r^2}{2}\right) + \frac{m}{q}azr\cos(\theta + \omega_r t), \tag{3}$$

where ω_r is the drive frequency and a is related to the amplitude of the potential. Assuming that the cooling can be described by a Stokes viscous drag, i.e. there is a friction term proportional to the velocity of the particle with κ being the constant of proportionality, the equations of motion are then given by

$$\begin{aligned}
\ddot{x} &= \frac{\omega_z^2}{2}x - az\cos(\omega_r t) + \Omega_c\dot{y} - \kappa\dot{x},\\
\ddot{y} &= \frac{\omega_z^2}{2}y + az\sin(\omega_r t) - \Omega_c\dot{x} - \kappa\dot{y},\\
\ddot{z} &= -\omega_z^2 z - a[x\cos(\omega_r t) - y\sin(\omega_r t)] - \kappa\dot{z}.
\end{aligned} \tag{4}$$

Changing to a rotating coordinate system defined by $\boldsymbol{V}^{\pm} = \dot{\boldsymbol{r}} + \omega_{\mp}\hat{\boldsymbol{z}} \times \boldsymbol{r}$ (for more details see the review by Brown and Gabrielse [30]) decouples the magnetron (−) and cyclotron (+) motions, so equation (4) transforms to

$$\dot{V}_x^{\pm} = \omega_{\pm}V_y^{\pm} - \kappa\left[V_x^{\pm} + \frac{\omega_{\mp}}{\omega_+ - \omega_-}(V_x^+ - V_x^-)\right] - az\cos(\omega_r t), \tag{5a}$$

$$\dot{V}_y^{\pm} = -\omega_{\pm}V_x^{\pm} - \kappa\left[V_y^{\pm} + \frac{\omega_{\mp}}{\omega_+ - \omega_-}(V_y^+ - V_y^-)\right] + az\sin(\omega_r t), \tag{5b}$$

$$\ddot{z} = -\omega_z^2 z - \kappa\dot{z} - \frac{a}{\omega_+ - \omega_-}\left[(V_y^- - V_y^+)\cos(\omega_r t) - (V_x^+ - V_x^-)\sin(\omega_r t)\right]. \tag{5c}$$

As will be shown, the maximum compression rate occurs when the drive frequency is equal to $(\omega_z + \omega_-)$, which according to equation (2) is much smaller than ω_+. This effectively decouples the magnetron and cyclotron motions, so the latter can be neglected [30]. Furthermore, because $\omega_- \ll \omega_+$ the friction terms in (5*a*) and (5*b*) can be neglected, giving rise to the following simplification:

$$\begin{aligned}
\dot{V}_x^- &= -\omega_- V_y^- - az\cos(\omega_r t),\\
\dot{V}_y^- &= \omega_- V_x^- + az\sin(\omega_r t),\\
\ddot{z} &= -\omega_z^2 z - \kappa\dot{z} + \frac{a}{\omega_+ - \omega_-}\left(V_y^-\cos(\omega_r t) + V_x^-\sin(\omega_r t)\right).
\end{aligned} \tag{6}$$

The analytical solution to these equations [29] shows that the particle magnetron radius approaches zero with a compression rate, Γ, given by

$$\Gamma = \frac{\kappa}{4}\left(1 - \sqrt{\frac{(\omega_r - \omega_0)^2}{\delta^2 + (\omega_r - \omega_0)^2}}\right), \tag{7}$$

where $\omega_0 = \omega_z + \omega_-$ and the width, δ, is dependent on the applied rotating wall amplitude and trap parameters via

$$\delta = \frac{a}{\sqrt{(\omega_+ - \omega_-)\omega_z}}. \tag{8}$$

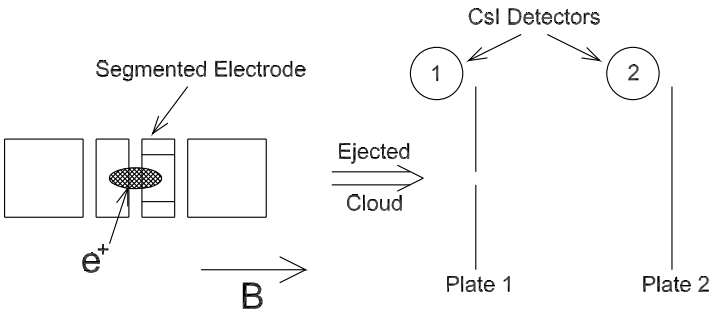

Figure 1. Schematic diagram of the measurement system. The hole radius in plate 1 is 1 mm.

3. Experimental details

As discussed in section 1, the experimental apparatus used for this study has been adapted from Swansea's pre-existing two-stage accumulator described in detail elsewhere [4] with significant equipment changes highlighted where relevant below. Previously, a 27 mCi (1 GBq) ^{22}Na source and a solid neon moderator provided a quasi-mono-energetic beam of (3–4) $\times$ 10^6 e^+s^{-1} to the positron accumulator located 2 m downstream. Currently, a 16 mCi ($\sim$0.6 GBq) source is employed but due to improvements in efficiency and technique, a comparable number of positrons are still available for accumulation via a similar approach. With respect to the apparatus, the main variation between that used here and previously [4] is the replacement of a 49 mm length second-stage electrode with a four-quadrant azimuthally segmented electrode and another shorter, cylindrical electrode (see figure 1). Each has an axial length of 24 mm, resulting in no overall change to the accumulator dimensions (the additional 1 mm being occupied by the electrical isolation provided by the sapphire spheres positioned between the electrodes). Attached to each segment is a voltage source that permits the application of a static potential, required for establishing the accumulation trap, combined with oscillating potentials, which give rise to the time-dependent radial potential of the rotating wall. The sinusoidal signals, produced by the two channels of an NF Wavefactory multichannel synthesizer (each channel having an initial phase difference of 90°), were split by standard 180° phase splitters to give the four components (0°, 90°, 180° and 270°) of the sinusoidal potential required. As also stated in section 1, it is necessary to provide an additional (to the nitrogen buffer that promotes capture into the trap) cooling gas within the second stage when the rotating wall is applied. To facilitate this, a further gas inlet has been installed in the second pumping box. The pressure, measured using a cold cathode Penning gauge, was typically (1–70) $\times$ 10^{-6} mbar and varied by $\lesssim$5% over a measurement period of hours. Because the nitrogen gas is inserted in the first stage, the nitrogen pressure in the second stage is about a factor of 5 higher than measured externally in the pumping box, based on pressure gradient calculations [31].

After accumulation and optional subsequent compression, the positrons were released by lowering the gate electrode, whereupon one of two detection methods was employed. The first method was to view the positron dumps on a phosphor screen with a charge-coupled device (CCD) camera which permitted many aspects of the resulting cloud to be determined, including the total number of particles it contained, its radial size and density profile. However, this technique suffered from a low signal-to-background ratio. The inability to synchronize the CCD

measurement with positron ejection resulted in the CCD signal being integrated over the whole measurement (up to 2000 s in many cases) while being exposed to the effect of the continuous high-energy positron beam from the source incident upon the phosphor screen. A background image had to be taken and subtracted to reveal the signal due to the release of the clouds.

The second method is depicted in figure 1. Ejected positrons on a trajectory with a radius larger than that of the hole (r_0) annihilate on plate 1, whereas the remaining positrons will reach plate 2. The number of positrons, N_1 and N_2, respectively, are derived from the recordings of the annihilation signals observed by the thallium-doped, caesium iodide crystals attached to a photosensitive PIN diode and preamplifier.

The magnetron kinetic energy, E_m, of the particles with magnetron amplitude, A_m, is given by

$$E_m = \tfrac{1}{2} m \omega_m^2 A_m^2. \tag{9}$$

Assuming that the particles are non-interacting and thermal, the radial distribution of the magnetron orbits, $N(r)$, is given by

$$N(r) \propto \exp\left(-\frac{E_m}{k_B T}\right) \propto \exp\left(-\frac{m\omega_m^2 A_m^2}{2k_B T}\right), \tag{10}$$

i.e. a Gaussian shape. It has been shown [32] that the width, σ, of the Gaussian can then be derived using

$$\sigma = \frac{r_0}{\sqrt{2\ln(1 + N_2/N_1)}}. \tag{11}$$

Measurements have shown that both methods gave the same width of the positron clouds, validating the assumption mentioned above.

4. Results and discussion

4.1. Commentary

As mentioned in section 3, nitrogen is used as the main buffer gas in the accumulator. A fortuitous feature of positron scattering from this molecule is the strong onset of the cross-section for electronic excitation above about 9 eV, which competes effectively with positronium formation (which is, in effect, a positron absorption channel). This has recently been observed directly [33] and has been implied indirectly for many years by traditional positron lifetime investigations (see, e.g., [34] for a description of this technique) that found that N_2 has an anomalously low positronium yield [35, 36]. The net effect is that N_2 is the optimum gas to promote positron capture into the accumulator, such that its presence is a prerequisite for the efficient operation of these devices.

However, it has also been known for many years, again from positron lifetime measurements, that, among the molecular gases, nitrogen is the poorest positron cooler, with the lowest density-normalized cooling rate or the longest thermalization time [37–40]. Thus, if a rapid cooling is required, which is the case here when the rotating wall is used, a further gas must be inserted into the system. Investigations have revealed that several gases have thermalization times about 100 times shorter than N_2 [40], such that addition of small quantities of these to the lowest potential region of the accumulator will promote positron cooling. SF_6 is one such gas, and this has been used in this study and in previous work [14, 22, 26]. We have also studied the effects of using CO_2 instead of SF_6 as a cooling gas during rotating wall compression.

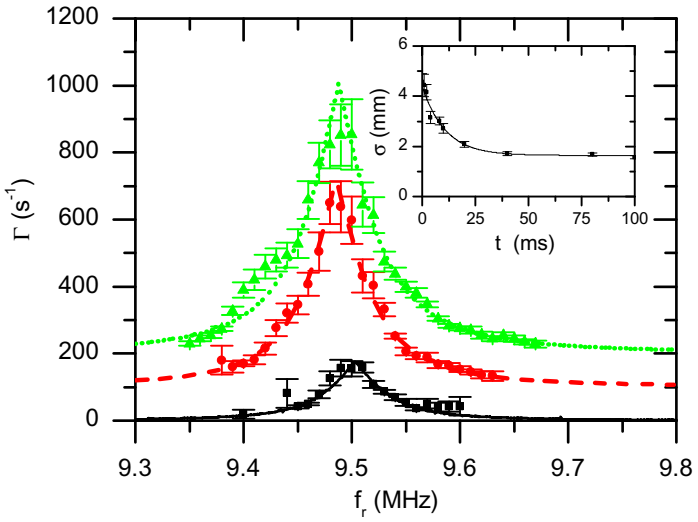

Figure 2. Compression rate as a function of the rotating wall frequency for the amplitudes of 75 mV (■) and 150 mV (●) offset by 100 s^{-1} and the amplitude of 225 mV (▲) offset by 200 s^{-1}. The line is fitted using equation (7). Inset: ejected cloud radius versus the rotating wall on-time; the line is a fit to equation (12). The uncertainties on the points in both graphs are due to scatter on repeated measurements.

4.2. Rotating wall compression after accumulation

About 10^4 positrons were accumulated in 100 ms with the rotating wall switched off. Subsequently, the accumulation was stopped and the rotating wall applied for a time t, after which the positrons were ejected from the trap and detected as described in section 3. The cloud radius, calculated via equation (11), can then be plotted versus t and the resulting compression curve (see the inset of figure 2) fitted using

$$\sigma(t) = (\sigma_0 - \gamma/\Gamma)\exp(-\Gamma t) + \gamma/\Gamma. \tag{12}$$

Here, σ_0 is the width of the cloud at $t = 0$. The origin of the coefficient γ is not yet understood, but it is likely to be related to collisions with the buffer and cooling gases and the presence of trap field asymmetries, both of which are known to cause cloud expansion, at least in the plasma regime [41, 42].

The main graph in figure 2 shows the compression rate as a function of the applied rotating wall frequency, f_r, for three different amplitudes. The lines are fits to equation (7). The figure shows that there is very good agreement with the theory.

Equation (8) predicts that the width of the compression curves shown in figure 2 is proportional to the applied peak-to-peak rotating wall voltage, V_r, which is corroborated by the measurements, with rotating wall amplitudes between 75 and 600 mV, as can be seen in figure 3. Using equation (3), it can be shown that $V_r = (m/q)af$, with f being a geometrical trap factor. This factor can be estimated by approximating the electrical potential in the trap using two first order (in r and z) Taylor expansions to yield a value of $\sim$61 kHz V^{-1}. The fitted gradient of 134 ± 15 kHz V^{-1} is clearly higher; moreover, the fitted line has an offset. These discrepancies with theory can be attributed to the anharmonic nature of the potential well for particles

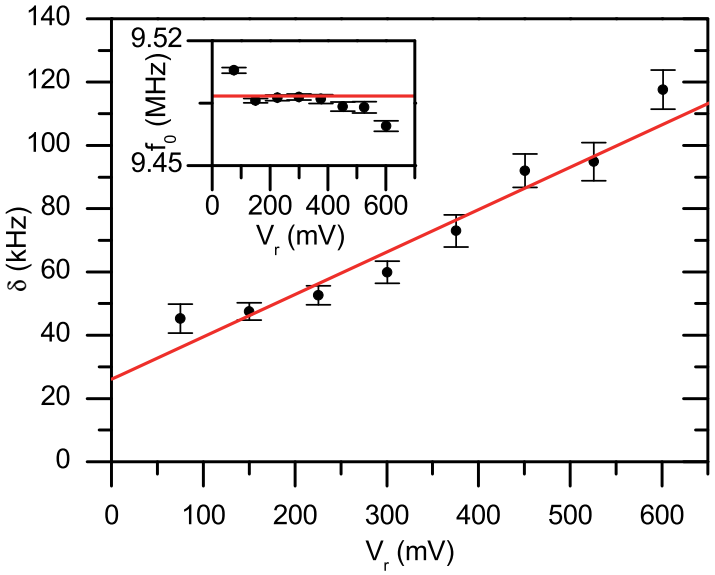

Figure 3. Frequency response width versus the applied rotating wall amplitude with a fitted gradient of $134 \pm 15\,\mathrm{kHz\,V^{-1}}$ and an offset of $26.1 \pm 4.5\,\mathrm{kHz}$. The inset shows that the central frequency of the response curve ($f_0 = \omega_0/2\pi$) remains more or less constant across this range of amplitudes with a mean value of $9.4889 \pm 0.0030\,\mathrm{MHz}$, which is in excellent agreement with the calculated value of 9.49 MHz [29]. The uncertainties are derived from the fits to equations (7) and (8).

with higher energies. Assuming a cloud temperature equivalent of approximately 55 meV, a numerical evaluation of bounce frequencies followed by a convolution with equation (7) reproduces an offset consistent with that in figure 3, whereas the shape of the compression curves does not change significantly. Moreover, assuming that there is a linear relationship between the rotating wall amplitude and the cloud temperature, the width of the compression curves increases with increasing amplitude. The larger slope can then be explained by assuming a temperature increase of 10 meV per applied volt.

Figure 4 shows a linear relationship between the pressure, and therefore the number density, of cooling molecules for a variety of rotating wall amplitudes. Naively, this is what should be expected considering the viscous drag model. However, the cooling of the positrons is provided by the low-energy inelastic scattering with SF_6 molecules where the scattering cross-section is assumed to be strongly energy-dependent near threshold, similar to that of CO_2 [43]. Assuming that the positron temperature is dependent on the pressure, it could be accidental that, as implied by figure 4, there is a linear relationship between the value of κ and the amount of SF_6 present. For instance, for an amplitude of 75 mV, κ is constant. More research is needed to gain a better understanding of these data, including the apparent low-pressure offset.

4.3. Accumulation without the rotating wall

The number of accumulated positrons, $N(t)$, after a time, t, can be described by

$$N(t) = N(\infty)(1 - \mathrm{e}^{-t/\tau}), \tag{13}$$

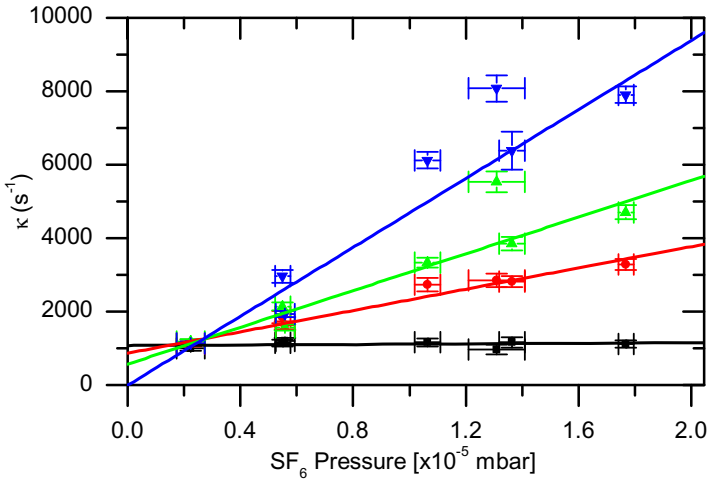

Figure 4. Friction coefficient, κ, versus SF_6 pressure for rotating wall amplitudes of 75 mV (■), 150 mV (●), 225 mV (▲) and 300 mV (▼). The lines are linear fits to the data.

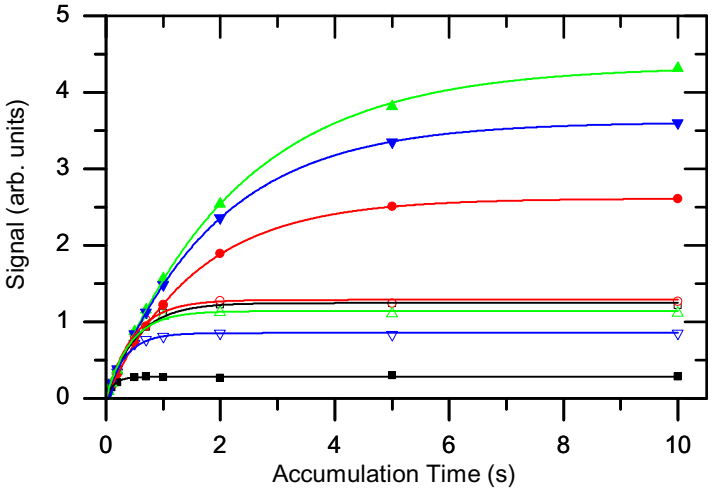

Figure 5. Some typical accumulation curves for a number of SF_6 gas pressures. The closed symbols represent measurements carried out when the rotating wall was on, with the open symbols for the rotating wall off. ■, 0 mbar; ● 10^{-6} mbar; ▼, 5×10^{-6} mbar; ▲, 2×10^{-5} mbar.

where τ is the positron lifetime in the trap and $N(\infty) = R\tau$, with R being the rate at which positrons from the low-energy beam are accumulated. A few examples of accumulation curves are shown in figure 5, where the open and closed symbols indicate whether the rotating wall is off or on, respectively, and the lines are fits to equation (13).

The value of τ is determined by annihilation on the N_2 buffer gas and the added cooling gas and, in the absence of the rotating wall, by collision-induced cross-field transport to the electrode walls via

$$\frac{1}{\tau} = \lambda_T = \lambda_{ann}^{N_2} + \lambda_{ann}^{cool} + \lambda_{cft}^{N_2} + \lambda_{cft}^{cool}, \tag{14}$$

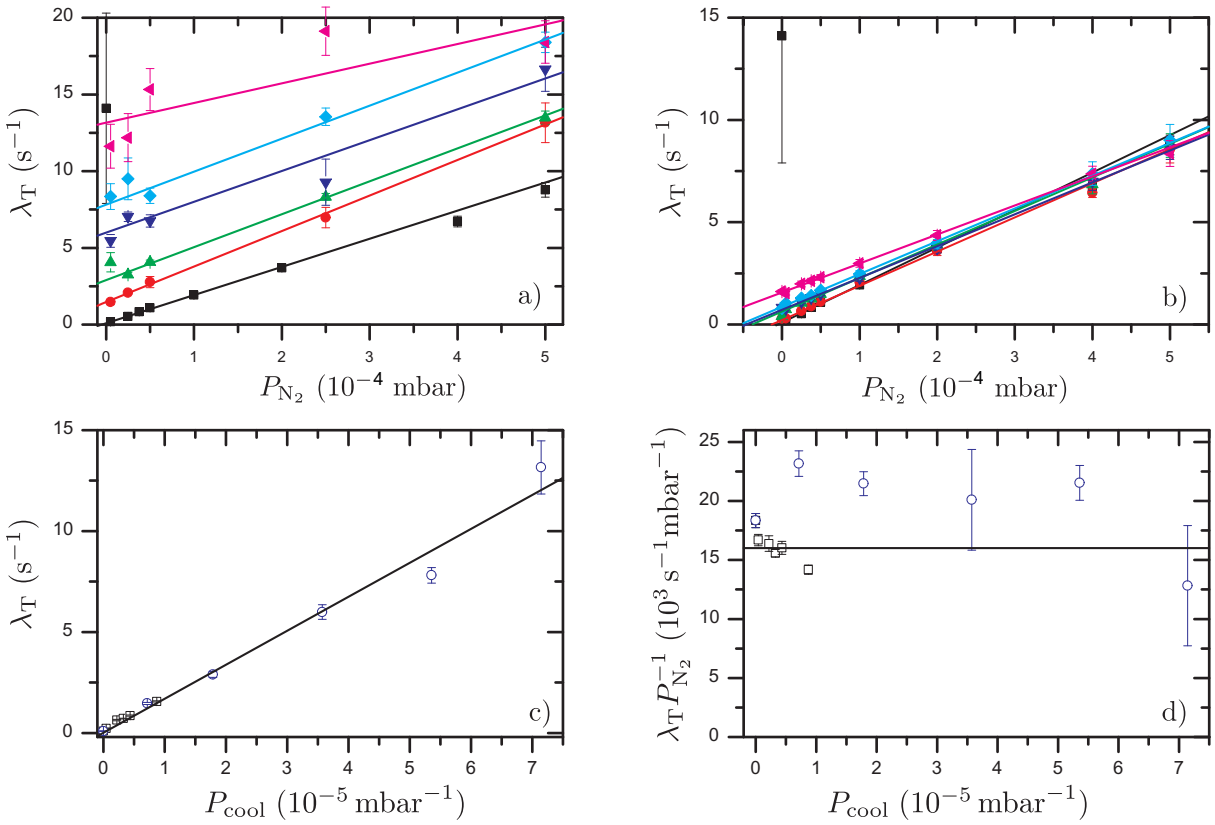

Figure 6. Comparison between CO_2 and SF_6 as the cooling gas. (a) Loss rate as a function of nitrogen pressure using CO_2 as cooling gas with pressures in units of 10^{-5} mbar: ■, 0; ●, 0.7; ▲, 1.8; ▼, 3.6; ♦ , 5.4; ◂, 7.1; the lines are linear fits to the measured points. (b) The same as (a) but for SF_6 with pressures in units of 10^{-6} mbar. ■, 0; ●, 0.4; ▲, 2.2; ▼, 3.3; ♦, 4.3; ◂, 8.7. (c) Annihilation rate for CO_2 (○) and SF_6 (□). The solid line is a linear fit. (d) Loss rate per mbar of N_2 derived from panels (a) and (b); symbols are as in (c).

where λ_T, λ_{ann} and λ_{cft} are the total, annihilation and cross-field transport loss rates, respectively, and the index cool indicates a cooling gas. The cross-field transport loss rate is known to be proportional to the neutral gas pressure for non-neutral plasmas [41], assumed here to behave in a similar fashion in the single-particle regime, and so is the annihilation rate. Therefore, equation (14) can be written as

$$\lambda_T = C P_{N_2} + D P_{cool}, \tag{15}$$

with C and D being constants and P_{N_2} and P_{cool} the nitrogen and cooling gas pressures, respectively.

In figures 6(a) and (b), the measured loss rates as a function of nitrogen pressure for a number of different SF_6 and CO_2 pressures are shown, where the lines depict linear fits to the data. The intercepts of the fitted lines for both gases are plotted in figure 6(c). The solid line is a linear fit, giving a value for $D \simeq 1.7 \times 10^5$ s^{-1} mbar^{-1}. Interestingly, D seems to be independent of the cooling gas type. Using standard values for the positron annihilation parameter, Z_{eff} [34], the annihilation rates for SF_6 and CO_2 are 1.8×10^4 and 9.6×10^3 s^{-1} mbar^{-1}, respectively,

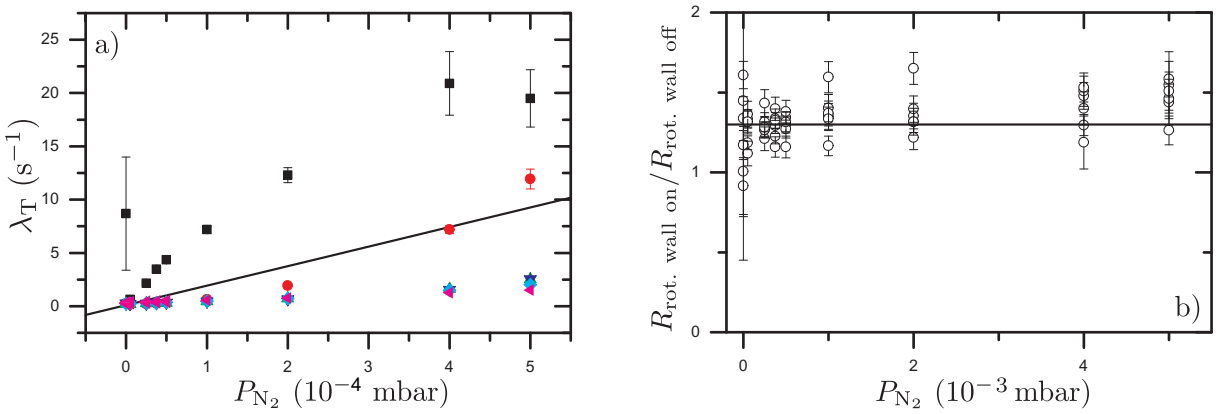

Figure 7. (a) Loss rate as function of the nitrogen pressure for different SF_6 pressures in units of 10^{-6} mbar: ■ 0; ● 0.4; ▲ 2.2; ▼ 3.3; ♦ 4.3, ◀ 8.7. The solid line represents the loss rate for 0 mbar without rotating wall applied. (b) Ratio of the trapping rates with rotating wall on and off for a number of different SF_6 pressures.

indicating that cross-field transport is a significant contributor (∼90% for these cooling gases) to the loss rate. The cross-field loss rate is likely dominated by experimental factors, such as the trap parameters that determine ω_z and the magnetic field strength, which may explain the lack of sensitivity to the cooling gas type. The fitted value of the offset at zero N_2 pressure, $0.135 \pm 0.022\ s^{-1}$, is probably caused by a combination of annihilation and transport on background gas molecules and asymmetries in the trap electric and/or magnetic fields.

The values of the fitted slopes in figures 6(a) and (b) are plotted in figure 6(d). There is little variation between the two cooling gases. The resulting value for $C \approx 1.6 \times 10^4\ s^{-1}\ mbar^{-1}$ is represented by the horizontal line in the figure.

4.4. Rotating wall compression during accumulation

Considering the accumulation curves for the rotating wall continuously applied as given in figure 5, a number of observations can be made. When the rotating wall is applied without an extra cooling gas the positron lifetime is reduced, so we can conclude that nitrogen alone cannot cool the positrons efficiently to counteract the increase in temperature caused by the rotating wall electric field, which presumably results in increased radial transport. Inserting a cooling gas with the rotating wall off lowers $N(\infty)$, which is caused mainly by radial transport since R is dependent on the value of P_{N_2} (see below) and not P_{cool}. However, switching on the rotating wall dramatically increases $N(\infty)$ and therefore the lifetime, implying that the loss rate, λ_T, is, as was concluded earlier (see also below), mainly due to radial transport and not positron annihilation. The last point is made clearer in figure 7(a) where the loss rate is plotted as a function of the nitrogen pressure for a number of SF_6 pressures. The line shows the fitted behaviour with only nitrogen gas present and the rotating wall off.

The data in figure 7(b) represent the ratio of R with rotating wall on and off. It is to be expected that this ratio is 1; however, the mean value of all measurements gives a value of about 1.3, as shown by the horizontal line in the figure. This is not yet understood, but may be a result of an increasing transport efficiency of positrons between the first and the second stage of the trap (see the discussion in [4]) caused by the rotating wall.

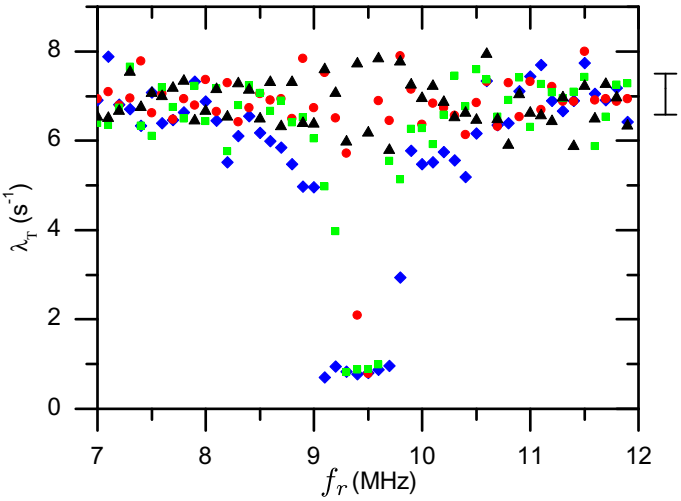

Figure 8. The measured loss rate from the trap with the rotating wall applied during the accumulation cycle as f_r is varied at fixed SF_6 pressure and for various amplitudes: 0 V (▲), 100 mV (●), 500 mV (■) and 1.0 V (◆). The error bar to the right of the figure represents the typical uncertainty around $\lambda_T = 8\,s^{-1}$, whereas the uncertainty for low values of λ_T is roughly the size of the points.

The behaviour of the loss rate with rotating wall frequency is shown in figure 8. Close to the central frequency the loss rate decreases to the expected annihilation rate, implying that the loss due to radial transport is cancelled by the rotating wall. The width of this low loss rate region increases with increasing amplitude.

The nitrogen gas pressure of 1×10^{-4} mbar combined with the SF_6 pressure of 9×10^{-6} mbar should give a loss rate of about $3\,s^{-1}$ with the rotating wall off based on the above measurements. The off-resonance loss rate is about $7\,s^{-1}$, showing that the rotating wall affects the loss rate, probably by imparting extra energy to the positron cloud. The combined annihilation rate is estimated to be $0.7\,s^{-1}$, which is very close to the minimum value of about $0.75\,s^{-1}$ at the resonance frequency.

5. Conclusion

We have presented a comprehensive study of the effect of an asymmetric rotating dipole electric field, applied at a frequency close to that of the axial bounce motion, on a cloud of positrons in the single-particle regime in a two-stage accumulator. Investigations have been performed with the rotating wall off, switched on after accumulation is complete and present during accumulation. We have observed that the rotating wall enhances the lifetime and thus the number of accumulated positrons when cooling gas is added (SF_6 and CO_2 were studied). This has been attributed to the elimination of collision-induced radial transport by the rotating wall, which acts to compress the positron cloud. Compression rates have been presented that are adequately described by analytical theory, which models the role of the cooling gas using a Stokes viscous drag term. Peak compression rates close to $10^3\,s^{-1}$ have been found, such that clouds can be rapidly compressed using this technique for extraction from the trap and for subsequent applications. The positron cloud radius was found to be limited to just below 2 mm. This was

attributed to the effects of collision-related expansion, although further studies of the origins of this limit are warranted.

Acknowledgments

We are grateful to Dr Rod Greaves of First Point Scientific Inc. for communicating the results of his study prior to publication and for numerous helpful discussions over the years. We thank the EPSRC for their support of the positron physics and antihydrogen programme at Swansea, currently via awards EP/E048951/1 and EP/H026932/1 and via studentships to CJB, CAI and SJK. DPvdW is grateful to RCUK for the provision of a fellowship.

References

[1] Surko C M, Passner A, Leventhal M and Wysoki F J 1988 *Phys. Rev. Lett.* **61** 1831
[2] Murphy T J and Surko C M 1992 *Phys. Rev.* A **46** 5696
[3] Greaves R G and Surko C M 2004 *Phys. Plasmas* **11** 2333
[4] Clarke J, van der Werf D P, Griffiths B, Beddows D C S, Charlton M, Telle H H and Watkeys P R 2006 *Rev. Sci. Instrum.* **77** 063302
[5] Cassidy D B, Deng S H M, Greaves R G and Mills A P Jr 2006 *Rev. Sci. Instrum.* **77** 073106
[6] Sullivan J P, Jones A, Caradonna P, Makochekanwa C and Buckman S J 2008 *Rev. Sci. Instrum.* **79** 113105
[7] Amoretti M *et al* (ATHENA Collaboration) 2002 *Nature* **419** 456
[8] Jørgensen L V *et al* (ATHENA Collaboration) 2005 *Phys. Rev. Lett.* **95** 025002
[9] Gabrielse G *et al* (ATRAP Collaboration) 2002 *Phys. Rev. Lett.* **89** 213401
[10] Andresen G B *et al* (ALPHA Collaboration) 2011 *Phys. Lett.* B **695** 95
[11] Andresen G B *et al* (ALPHA Collaboration) 2010 *Nature* **468** 673
[12] Andresen G B *et al* (ALPHA Collaboration) 2011 *Nature Phys.* **7** 558
[13] Gabrielse G *et al* (ATRAP Collaboration) 2012 *Phys. Rev. Lett.* **108** 113002
[14] Cassidy D B, Deng S H M, Greaves R G, Maruo T, Nishiyama N, Snyder J B, Tanaka H K M and Mills A P Jr 2005 *Phys. Rev. Lett.* **95** 195006
[15] Cassidy D B and Mills A P Jr 2007 *Nature* **449** 195
[16] Dubin D H E and O'Neil T M 1999 *Rev. Mod. Phys.* **71** 87
[17] O'Neil T M 1999 *Phys. Today* **52** 24
[18] Schauer M, Mitchell T and Nebel R (ed) 2003 *AIP Conf. Series of Non-Neutral Plasma Physics V* (CP692) (New York: AIP)
Drewsen M, Uggerhøj U and Knudsen H (ed) 2006 *AIP Conf. Series of Non-Neutral Plasma Physics VI* (CP862) (New York: AIP)
Danielson J R and Pedersen Th S (ed) 2008 *AIP Conf. Series Non-Neutral Plasma Physics VII* (CP1114) (New York: AIP)
[19] Huang X P, Anderegg F, Hollmann E M, Driscoll C F and O'Neil T M 1997 *Phys. Rev. Lett.* **78** 875
[20] Anderegg F, Hollmann E M and Driscoll C F 1998 *Phys. Rev. Lett.* **81** 4875
[21] Greaves R G and Surko C M 2000 *Phys. Rev. Lett.* **85** 1883
[22] Danielson J R and Surko C M 2005 *Phys. Rev. Lett.* **94** 035001
[23] Danielson J R, Surko C M and O'Neil T M 2007 *Phys. Rev. Lett.* **99** 135005
[24] Danielson J R and Surko C M 2006 *Phys. Plasmas* **13** 055706
[25] Watson T L 1999 Accumulation and manipulation of positron plasmas for antihydrogen production *PhD Thesis* University of Wales, Swansea
[26] Greaves R G and Moxom J 2008 *Phys. Plasmas* **15** 072304

[27] Sullivan J P, Makochekanwa C, Jones A, Caradonna P and Buckman S J 2008 *J. Phys. B: At. Mol. Opt. Phys.* **41** 081001
[28] Weber T R, Danielson J R and Surko C M 2008 *Phys. Plasmas* **15** 012106
[29] Isaac C A, Baker C J, Mortensen T, van der Werf D P and Charlton M 2011 *Phys. Rev. Lett.* **107** 033201
[30] Brown L S and Gabrielse G 1986 *Rev. Mod. Phys.* **58** 233
[31] Watkeys P R 2008 Towards laser excitation of positronium and advances in positron accumulation techniques *PhD Thesis* University of Wales, Swansea
[32] Isaac C A 2011 Axialisation of particles in a Penning-type trap by the application of a rotating dipole electric field and its application to positron accumulation *PhD Thesis* University of Wales, Swansea
[33] Marler J P and Surko C M 2005 *Phys. Rev.* A **72** 062713
[34] Charlton M and Humberston J W 2001 *Positron Physics* (Cambridge: Cambridge University Press)
[35] Schrader D M and Svetic R E 1982 *Can. J. Phys.* **60** 517
[36] Charlton M 1985 *Rep. Prog. Phys.* **48** 737
[37] Griffith T C and Heyland G R 1978 *Phys. Rep.* **39** 169
[38] Paul D A L and Leung C Y 1968 *Can. J. Phys.* **46** 2779
[39] Coleman P G, Griffith T C and Heyland G R 1981 *J. Phys. B: At. Mol. Opt. Phys.* **14** 2509
[40] Al-Qaradawi I, Charlton M, Borozan I and Whitehead R 2000 *J. Phys. B: At. Mol. Opt. Phys.* **33** 272
[41] Malmberg J H and Driscoll C F 1980 *Phys. Rev. Lett.* **44** 654
[42] Notte J and Fajans J 1994 *Phys. Plasmas* **1** 1123
[43] Surko C M, Gribakin G F and Buckman S J 2005 *J. Phys. B: At. Mol. Opt. Phys.* **38** R57